PROCEEDINGS, Thirty-Fourth Workshop on Geothermal Reservoir Engineering
Stanford University, Stanford, California, February 9-11, 2009
SGP-TR-187

DETAILED IMAGE OF FRACTURES ACTIVATED BY A FLUID INJECTION IN A PRODUCING INDONESIAN GEOTHERMAL FIELD

Gillian R. Foulger[1] & Luciana De Luca[2]

[1]Dept. Earth Sciences, University of Durham,
Science Laboratories, South Rd.,
Durham, DH1 3LE, U.K.
email: g.r.foulger@durham.ac.uk

[2]WesternGeco EM – Geosystem,
Via Clericetti, 42/A,
20133 Milan, Italy
email: ldeluca@milan.westerngeco.slb.com

ABSTRACT

We used several data-processing techniques to analyze 237 earthquakes in order to study a water injection experiment in a geothermal field in Indonesia. We calculated an optimal *a-priori* one-dimensional crustal model by inverting the entire set of *P*- and *S*-wave arrival time measurements. The relocated earthquakes formed a tight cluster near the bottom of the injection well. These locations provide the best estimate of the absolute location of the cluster. We computed relative hypocenter locations from arrival-time differences using the program *hypocc*, which spectacularly improved the clustering of the locations. The earthquakes defined a planar structure striking N 50˚ E and dipping 70˚ to the NW. It was ~ 400 m long (along strike) and ~ 400 m high (down dip). We derived moment tensors for 38 earthquakes by inverting body-wave amplitude ratios. Most had large explosive components and were consistent with combined tensile crack opening and shear. Most were consistent with both components responding to the same stress field, but a significant number, including some of the largest earthquakes, required different orientations for the stress fields, corresponding to the opening and shear components. A component of fluid inflow into the newly formed crack at the moment of rupture is also required to fit the data. A joint interpretation of the results provides a detailed picture of the effect of water injection into the well. The water flowed into a pre-existing fault zone, part of which was activated seismically by a tiny foreshock followed immediately by a large M 3.3 earthquake. This large earthquake affected some tens of metres of the fault, causing opening at the millimetre level, combined with shear slip. Failure in this mode then propagated out over a ~ 400 x 400-m plane via many more smaller earthquakes. The activated plane represents part of a more extensive fault zone.

INTRODUCTION

We analysed microearthquake data from a producing geothermal field in Indonesia. The field lies within an active Quaternary volcanic region that includes several historically active volcanic centers. The geothermal field is one of several within a broad geothermal province in West Java (Indonesia). The potential for energy generation from the province is estimated to be several thousand MWe.

As part of ongoing developments to increase production in the field, an injection well was recently drilled. Microearthquake surveys have been conducted to map fluid migration paths during well testing and/or re-injection of brines from steam condensate.

Microearthquake monitoring can detect permeability structures created or activated by stimulations in geothermal reservoirs. They may be induced both by pore pressure and thermal changes, *e.g.*, as a result of the interaction of circulating reservoir fluids and hot rocks [Foulger and Long, 1984]. With the exception of regions penetrated by drilling, the recognition and characterization of fluid paths can essentially only be done using microearthquake analysis, since this is one of only few methods available to locate fault zones precisely. High-quality results require recording microearthquakes on a well-designed, high-quality seismometer network.

State-of-the-art microearthquake data analysis involves calculation of accurate hypocentral locations, crustal velocity models, and moment

tensors. The latter is a mathematical description of the forces at work at the source, that allows crack-opening components to be expressed in addition to the shear motions that occur on planar faults. Careful analysis can reveal fault geometry, microearthquake source mechanisms, and details of the deformation that accompanied the microearthquake sequence. This information can be correlated with production/exploitation activities in the reservoir, and it can provide valuable information to help make decisions regarding the siting of new producer wells.

DATA ACQUISITION & PROCESSING METHODS

The microearthquake survey was conducted between December 2007 and January 2008, to monitor a water/condensate injection experiment. Over a period of 11 days, injection was conducted at rates of 30-40 l/s. A 10-station, 24-bit, three-component surface seismic network of 1 Hz sensors was deployed around the injection well. The aperture of the network was ~ 8 km. This was chosen in the expectation that the induced microearthquakes would occur near the bottom of the injection well at ~ 1.5 km below the surface. Continuous data were recorded at a sampling rate of 200 samples/s for 44 days.

We computed a optimal one-dimensional crustal model for the area, as a pre-requisite to determining high-resolution relative hypocenter locations. Following this, we computed full moment tensors for the best-recorded microearthquakes.

RESULTS

The seismic rate was low up to December 22nd 2007, when it began to increase. Activity became vigorous December 23rd when a swarm of 73 earthquakes was recorded. This swarm started with an earthquake with a magnitude of M_L= -0.8. This was followed by the largest-recorded event which had a magnitude of M_L= 3.3. The most vigorous part of the swarm comprised 52 events, all of which occurred within about an hour. The seismic rate remained high until January 1st, 2008. The activity did not correlate either with the start of water injection or with any increase in injection rate. The first event occurred in the middle of the injection period when the rate was 40 l/s.

We calculated preliminary hypocenters for 237 earthquakes using *P*-and *S*-wave arrival times automatically picked, and subsequently refined manually (Figure 1, left). Fort this we used an *a-priori* one-dimensional velocity model. We subsequently optimized the velocity model by simultaneously inverting the *P*- and *S*-wave arrival times for the best-fitting one-dimensional crustal model and hypocentral parameters. We used the program *velest* [Kissling *et al.*, 1994] which inverts earthquake arrival-time data to calculate a velocity model parameterized as a stack of homogeneous layers (Figure 2).

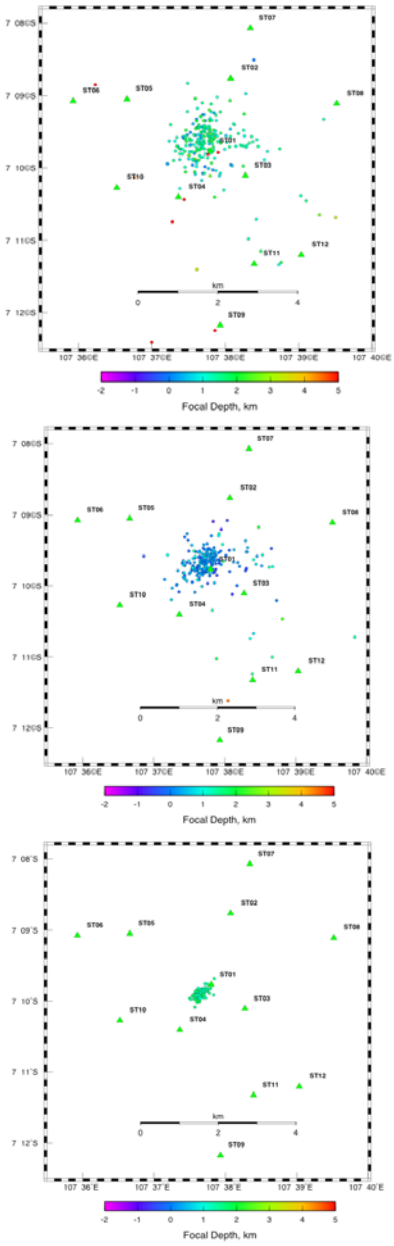

Fig. 1: Earthquake epicenter plots. Top: preliminary locations calculated using an a priori crustal model; Middle: locations calculated by one-dimensional simultaneous inversion using program velest; Bottom: relatively relocated epicenters calculated using program hypocc.

Substantially higher *P*-wave velocities were required by the data, for the upper ~ 3 km. An average value of *Vp/Vs* of 1.63 was obtained, with particularly low

values in the upper ~ 1.5 km. Such low values may result from steam in pores, geothermal alteration in the reservoir rocks, low pore pressures and/or steam domination.

Increasing crustal velocities in the shallow layers had the effect of shallowing the calculated hypocentral depths by an average of ~ 1.2 km. This result emphasizes the importance of a robust velocity model for microearthquake locations. The hypocenters calculated using the improved velocity model were more clustered than the preliminary locations, consistent with improvement in the accuracy of the locations (Figure 1, Top and Middle).

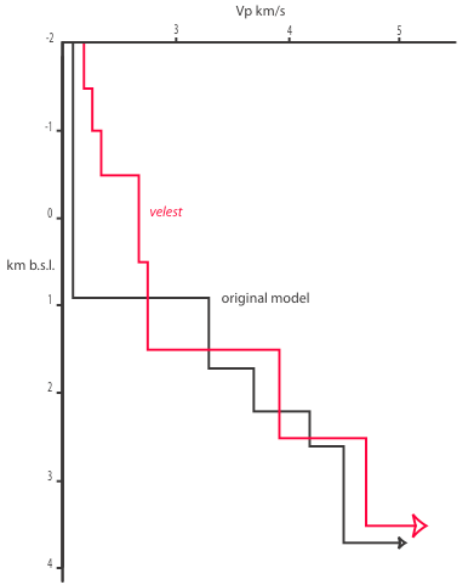

Fig. 2: Velocity-depth plot of a priori P-wave velocity model and the optimized one-dimensional model calculated using velest [Kissling et al., 1994].

RELATIVE HYPOCENTER RELOCATIONS

Traditional hypocenter location methods analyze one earthquake at a time, and are subject to biases caused by errors in the crustal velocity model. These biases can be reduced to some extent by improving the crustal model and the picking accuracy. However, the relative relocation method is much more powerful to reduce *inter-earthquake* location errors by processing large sets of earthquakes simultaneously.

Relative relocation techniques divide the entire dataset into discrete clusters of closely grouped earthquakes. The members of each cluster are then relocated relative to one-another. This yields much higher resolution of the locations of earthquakes within a cluster relative to others in the same cluster. The preliminary hypocenters and optimized crustal velocity model were used for the relative relocation process. All 237 earthquakes were relocated. Initial refinements of the input data reduced the original set to a single cluster of 123 earthquakes. A significant improvement in location clustering was achieved for these earthquakes (Figure 1, right). The original ~ 1000 m x 500 m epicentral area shrank to a zone 400 m x 180 m in size. A linear feature striking N 50˚E immediately became obvious.

In the vertical direction, the hypocentral volume shrank from 1 km in depth extent to 400 m, revealing a feature dipping at ~ 70˚ to the northwest. The underside of the dipping structure is sharply defined, suggesting relative location accuracies of a few tens of meters (Figure 3).

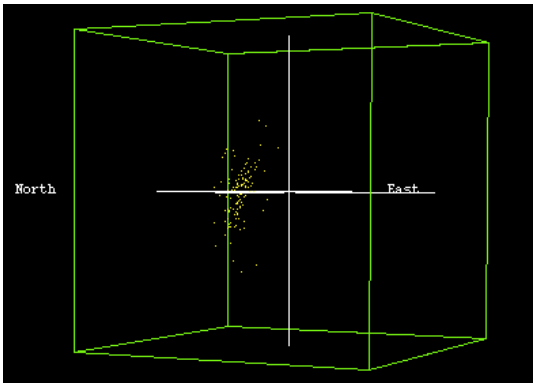

Fig. 3: Depth section showing the microearthquake hypocenters calculated using relative relocations. The direction of sight is N 50˚E. The green box is 2 x 2 x 2 km in size.

MOMENT TENSORS

Moment tensors were calculated using the method of Julian and Foulger [1996]. This involves determining the best-fit symmetric moment tensor for a set of measured *P*-, *SH*- and *SV*-phase polarities and *P:SH*, *P:SV*, and *SH:SV* amplitude ratios. The optimized one-dimensional crustal model was used.

The data were well suited to moment tensor inversion because the seismic network had been optimally designed and the quality of the recordings was excellent. Moment tensors for 38 earthquakes were successfully derived. Examples of typical mechanisms are shown in Figure 4, and source types and source orientations for the entire dataset are shown in Figure 5.

Many of the earthquakes lie in source-type space between the ±Dipole mechanisms (Figure 5, Top). Most have large explosive components. Only a few relatively poorly constrained earthquakes had significant implosive components or plot near to the

DC point. A second distribution extends from the +Dipole point horizontally across the plot. These sources have large volumetric components but variable CLVD components.

The source orientation plot (Figure 5, Bottom) shows that the preferred orientation of the T-axes (indicative of the direction of σ_3) is NW-SE and sub-horizontal. For shear sources, this is consistent with right-lateral strike-slip on NS faults, or left-lateral strike-slip on EW-striking faults. It is also consistent with normal faulting on NE-striking faults. The P-axes (indicative of the direction of σ_1) vary in orientation from sub-horizontal NE-SW, up to vertical. For shear faulting, this would correspond to variation from strike-slip to normal faulting.

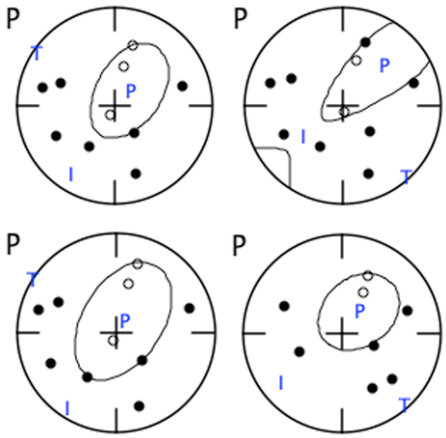

Fig. 4: P polarity plots in upper-hemisphere, equal-area projection showing the moment tensors of four typical earthquakes. These mechanisms resemble normal-faulting mechanisms with reduced dilatational fields (i.e., they have net explosive mechanisms). P, T and I indicate the pressure, tension and intermediate axes.

INTERPRETATION

Interpretation of moment tensors is ambiguous. In theory, a given moment tensor could correspond to an infinite number of physical source processes. However, the number of geologically reasonable interpretations is limited. The moment tensors typically obtained for geothermal earthquakes are well explained by cracking involving a combination of shear and crack opening/closing components.

Pure opening/closing cracks plot at the ±Crack positions in source-type space. ±Dipole sources have somewhat reduced volumetric components. The earthquakes that form a distribution extending from the +Dipole point toward the DC point can be explained by combinations of tensile cracks and shear wing faults, with small amounts of compensating fluid flow into the crack at the time of formation (Figure 6). This might be provided by the flow of fluid into the opening crack.

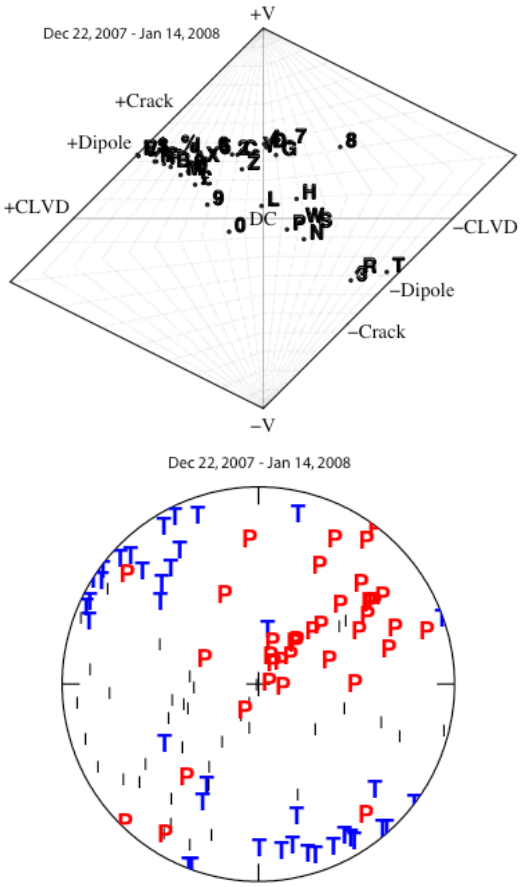

Fig. 5: Results of moment tensor inversion of the 38 best-recorded earthquakes. Top, source-type plot [Hudson et al., 1989; Julian et al., 1998]. This displays the results free of orientation information. Pure explosions plot at the top of the diagram, pure implosions at the bottom, and positive/negative CLVD sources at left/right. Double couple sources, consistent with shear slip on planar faults, plot at the point labeled DC in the middle of the diagram. Bottom: Equal area plot showing P-, I-, and T-axes. The P axes given an approximate indication of the direction of σ_1, the I axes σ_2 and the T axes σ_3.

The earthquakes whose moment tensors plot between the ±Crack and DC points may be interpreted as crack/shear-fault combinations where the normals to the planes of the two components lie in the same

plane (Figure 6). Earthquakes whose moment tensors plot on a horizontal line extending from the +Crack point toward the right and from the -Crack to the left may be interpreted as crack/shear-fault combinations where the shear fault is tilted with respect to the crack.

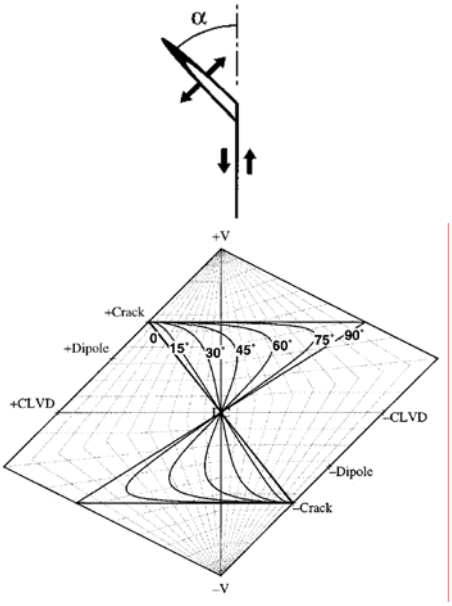

Figure 6: Top: Schematic figure showing a combined tensile and shear-faulting source, where both components represent failure in response to the same stress-field orientation. Bottom: Diagram illustrating where such sources would plot in source-type space. Where the normals to the shear and tensile components lie in the same plane, the sources plot between the ±Crack and DC points along the line labeled "0°". Where normals to the shear and tensile components lie at an angle, the sources plot to the right of this line. Numbers labeling contours indicate the angles between the normals to the tensile and shear fault planes [from Julian et al., 1998].

Ambiguity in the orientation of the crack and shear components can be reduced by using the orientation of the structure revealed by the relative relocations. These showed that the earthquakes delineated a planar structure striking at ~ N 50˚ E and dipping at ~ 70˚ to the NW. Such a plane is superimposed on the source-orientation plot in Figure 7. The projection of the structure lies very close to the main zone of P axes that trends from sub-horizontal NE-SW up to vertical.

If this structure represents a shear-slipping fault with mechanisms ranging from normal to strike-slip, the P-axes would plot at 45˚ from it and their locus would comprise a small circle whose center projects at 20˚ from the perimeter of the plot (red line in Figure 7). In contrast, if the structure represents a pure opening crack, the P axes would project along the crack itself.

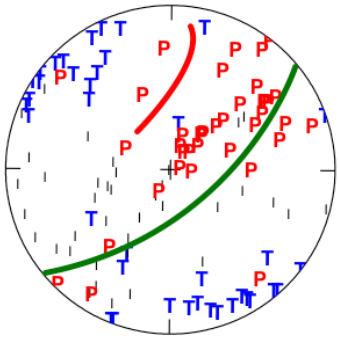

Figure 7: Source orientation plot for the moment tensors. Green line: upper hemisphere projection of a fault striking at N 50˚ E and dipping at 70˚ to the NW, similar to that imaged by the relative relocations. Red line: locus of P axes expected if the fault failed in a shear sense. If the fault failed as a tensile crack, the P axes are expected to lie along the projection of the fault (green line).

These results suggest that the main activated structure corresponds to the opening crack components of the individual earthquakes and that the shear components correspond to wing faults oblique to the main trend. Strikes a few tens of degrees more easterly than the main activated structure would be consistent with the observations.

CONCLUSIONS

Application of the relative relocation technique to this data set produced a major improvement in definition of the seismically activated structure. A M_L=3.3 earthquake corresponds to a source with dimensions no larger than a few tens of meters. The entire activated zone was ~ 400 m by 180 m in area, however. This suggests that the earthquakes activated a patch on a pre-existing fault that might be considerably longer than the activated part.

Many of the earthquakes had large explosive components. Few had implosive components. This is consistent with the fact that the swarm was induced by active fluid injection which would be expected to force cracks open and not close them. Comparison of the NE-striking structure imaged by the relative relocations and the moment tensor results strongly suggested that the structure corresponds to an opening crack or zone of cracking.

REFERENCES

Foulger, G. R., and R. E. Long (1984), Anomalous focal mechanisms; tensile crack formation on an accreting plate boundary, *Nature*, *310*, 43-45.

Hudson, J. A., R. G. Pearce, and R. M. Rogers (1989), Source type plot for inversion of the moment tensor, *J. geophys. Res.*, *94*, 765-774.

Julian, B. R., and G. R. Foulger (1996), Earthquake mechanisms from linear-programming inversion of seismic-wave amplitude ratios, *Bull. seismol. Soc. Am.*, *86*, 972-980.

Julian, B. R., A. D. Miller, and G. R. Foulger (1998), Non-double-couple earthquakes I. Theory, *Rev. Geophys.*, *36*, 525-549.

Kissling, E., W. L. Ellsworth, D. Eberhart-Phillips, and U. Kradolfer (1994), Initial reference models in local earthquake tomography, *J. geophys. Res.*, *99*, 19,635-619,646.